Ultrafast Gates for Single Atomic Qubits

W. C. Campbell,[*] J. Mizrahi, Q. Quraishi, C. Senko, D. Hayes, D. Hucul, D. N. Matsukevich, P. Maunz, and C. Monroe

Joint Quantum Institute, University of Maryland Department of Physics and National Institute of Standards and Technology,
College Park, Maryland 20742 USA

We demonstrate single-qubit operations on a trapped atom hyperfine qubit using a single ultrafast pulse from a mode-locked laser. We shape the pulse from the laser and perform a π rotation of the qubit in less than 50 ps with a population transfer exceeding 99% and negligible effects from spontaneous emission or ac Stark shifts. The gate time is significantly shorter than the period of atomic motion in the trap ($\Omega_{\mathrm{Rabi}}/\nu_{\mathrm{trap}} > 10^4$), demonstrating that this interaction takes place deep within the strong excitation regime.

PACS numbers: 03.67.Lx, 37.10.Vz, 37.25.+k

Quantum information processing requires the ability to perform operations in an amount of time shorter than the coherence time of the qubit. The ratio between coherence time and gate duration can be increased by improving coherence times or developing faster gates. One experimental extreme is found in atomic systems such as trapped ions, which can have coherence times of many minutes [1,2]. However, the precise spectral resolution needed to address narrow transitions and available excitation power have typically limited gate times to around a microsecond. In many condensed matter systems, on the other hand, single-qubit operations must be performed on picosecond time scales [3–6] owing to the short coherence time of the qubit ($T_2^* \leq 10$ ns in [3–6]). Here we realize ultrafast operations in an atomic system with very slow decoherence rates.

Aside from increasing the clock speed to decoherence rate ratio, there are also specific applications that would benefit immediately from fast single-qubit gates, such as noise-reduction techniques [7–10], entanglement of material qubits with photon time-bin qubits [11], and probabilistic gates with repetition rates limited by qubit rotations [12]. In particular, the ability to apply fast spin-dependent momentum kicks to trapped ions in the strong excitation regime [13] is a critical ingredient for fast sideband cooling [14] and fast entanglement of multiple atomic ion qubits [15,16]. Such entangling gates can be performed faster than a trap oscillation period, in contrast to motional gates using spectroscopically resolved sidebands.

We previously reported the implementation of an optical-frequency comb to perform qubit operations [17]. In the low excitation regime, each pulse alters the atomic state by a tiny amount and the effect of the pulse train is manifested through careful coherent accumulation of spectral density into narrow comb teeth, resulting in gate times of order 100 μs. In this Letter, we realize the strong excitation regime ($\Omega_{\mathrm{Rabi}} \gg \nu_{\mathrm{trap}}$) [13] and demonstrate fast control of an atomic qubit by driving stimulated Raman transitions with a single pulse from a picosecond mode-locked laser. In order to implement a fast π pulse, we perform simple pulse shaping in the form of a beam

splitter and delay line [18] to fully rotate the qubit in less than 50 ps with population transfer exceeding 99%. Since the atomic qubit is well isolated from its environment, the time required to perform such a fast gate is only a small fraction ($< 10^{-8}$) of the measured coherence time of our qubit. By setting the delay to zero in a counterpropagating geometry, the transition probability becomes sensitive to the atomic motion, which is the first step toward implementing fast cooling [14] and fast entangling gates between multiple ions [15,16].

Our experimental apparatus is shown in Fig. 1(c). A ^{171}Yb$^+$ ion is trapped in a linear radio frequency Paul trap. The $m_F = 0$ "clock states" of the two $^2S_{1/2}$ hyperfine levels act as the basis states of our qubit separated in frequency by $\nu_{\mathrm{HF}} = 12.642\,815$ GHz. Doppler cooling, state preparation, and state detection are accomplished on
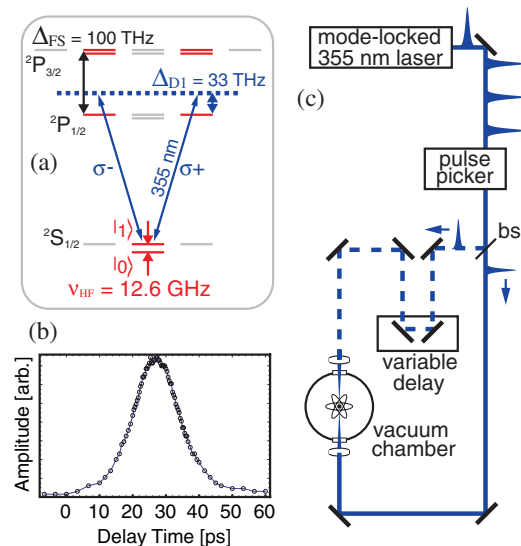

FIG. 1 (color online). Experimental schematic showing (a) the energy level diagram of ^{171}Yb$^+$ with relevant states (not to scale), (b) the envelope of the electric field autocorrelation from the mode-locked laser, and (c) the pulsed laser beam path with optional (dashed line) pulse-shaping beam path.

the $^2P_{1/2} \leftrightarrow {}^2S_{1/2}$ "D1 line" at 370 nm as described in Ref. [19]. The mode-locked laser for Raman transitions is a frequency-tripled yttrium vanadate laser operating at a repetition rate of $f_{\mathrm{rep}} = 121$ MHz with an average power of 4 W at 355 nm [20]. Single pulses are extracted by a Pockels cell pulse picker [21] and focused onto the ion.

Figure 1(a) shows the relevant energy levels of ^{171}Yb$^+$. The $^2S_{1/2}$ qubit states $|0\rangle$ and $|1\rangle$ are coupled through excited ^2P states via far-detuned light that is polarized to drive either σ^+ or σ^- transitions, as Raman transitions from π light are forbidden by selection rules. The $\sigma^\pm$ Raman transition (two-photon) Rabi frequency is [22,23]

$$\Omega_{0,1} = \pm \frac{g^2}{6}\left(\frac{1}{\Delta_{D1}} + \frac{1}{\Delta_{\mathrm{FS}} - \Delta_{D1}}\right), \qquad (1)$$

where g is the resonant one-photon Rabi frequency of the $^2P_{3/2}(F=2, m_F=2) \leftrightarrow {}^2S_{1/2}(F=1, m_F=1)$ "D2 line" cycling transition, Δ_{D1} is the detuning of the light above the $^2P_{1/2}$ state, $\Delta_{\mathrm{FS}} - \Delta_{D1}$ is the detuning of the light below the $^2P_{3/2}$ state, and $\Delta_{\mathrm{FS}} \approx 100$ THz is the fine-structure splitting. The ac Stark shifts of the qubit states from $\sigma^\pm$ light are [22,23]

$$\delta_0 = \frac{g^2}{12}\left(\frac{1}{\Delta_{D1}} - \frac{2}{\Delta_{\mathrm{FS}} - \Delta_{D1}}\right) \qquad (2)$$

$$\delta_1 = \frac{g^2}{12}\left(\frac{1}{\Delta_{D1} + \nu_{\mathrm{HF}}} - \frac{2}{\Delta_{\mathrm{FS}} - \Delta_{D1} - \nu_{\mathrm{HF}}}\right), \qquad (3)$$

where we have neglected the hyperfine splitting of the $^2P_{3/2}$ state.

Equations (1)–(3) show that if the Raman laser is tuned between the D1 and D2 lines ($0 < \Delta_{D1} < \Delta_{\mathrm{FS}}$) the stimulated Raman transition amplitudes due to the $^2P_{1/2}$ and $^2P_{3/2}$ couplings add constructively while the ac Stark shift contributions interfere destructively. The Stark shifts of the qubit states each cross zero near an optimal detuning of $\Delta_{D1}^{\mathrm{opt}} = \Delta_{\mathrm{FS}}/3$, which for Yb$^+$ corresponds to a Raman laser wavelength of $\lambda_{\mathrm{opt}} = 355$ nm. The differential ac Stark shift of the qubit states does not exactly cancel, but has a local minimum near λ_{opt}, reaching a value of $\delta_0 - \delta_1 \approx \Omega_{0,1}(3\nu_{\mathrm{HF}}/2\Delta_{\mathrm{FS}})$, corresponding to $2 \times 10^{-4}\Omega_{0,1}$ for Yb$^+$. We measure a differential Stark shift of $1.1(5) \times 10^{-4}\Omega_{0,1}$ through microwave Ramsey spectroscopy with linearly polarized 355 nm light.

The spontaneous emission rate can be estimated by calculating the excited state populations during the Raman transition to give [22,23]

$$\Gamma_{\mathrm{spon}} = \gamma \frac{g^2}{6}\left(\frac{1}{\Delta_{D1}^2} + \frac{2}{(\Delta_{\mathrm{FS}} - \Delta_{D1})^2}\right), \qquad (4)$$

where $\gamma \sim 2\pi \times 20$ MHz is the spontaneous emission rate from the ^2P states [24]. The probability of a spontaneous emission event during a π pulse near λ_{opt} can be estimated as $\mathcal{P}_{\mathrm{spon},\pi} \approx 3\gamma/2\Delta_{\mathrm{FS}}$. The local minima in Γ_{spon} and

$\mathcal{P}_{\mathrm{spon},\pi}$ lie close to λ_{opt} for Yb$^+$ at 349 nm and 352 nm, respectively. At 355 nm we estimate $\mathcal{P}_{\mathrm{spon},\pi} < 10^{-5}$.

We previously reported [25] resonant pulsed excitation of an atomic qubit out of the qubit manifold primarily to induce spontaneous emission for probabilistic photon-mediated entanglement. In contrast, here we demonstrate far off-resonant pulsed Raman transitions that manipulate the qubit itself for deterministic quantum gates. These gates must therefore have high fidelity and leave the state in the qubit manifold, which can be facilitated by using a Raman laser centered near λ_{opt}. For Yb$^+$, frequency-tripled mode-locked Nd:YAG and vanadate lasers are available that provide many Watts at a center wavelength of 355 nm [26].

The two-photon Rabi frequency in Eq. (1) is time dependent due to the shape of the pulse. As long as the pulse bandwidth is small compared to the single photon detunings Δ, the adiabatic elimination of the excited states remains valid and we can treat the qubit as a two-level system with a time-dependent coupling:

$$H_{\mathrm{eff}}/h = -\frac{\nu_{\mathrm{HF}}}{2}\hat{\sigma}_z - \frac{\Omega_{0,1}(t)}{2}\hat{\sigma}_x. \qquad (5)$$

Numerical solutions to the Schrödinger equation with this Hamiltonian can be obtained for a general time-dependent $\Omega(t)$. However, there is an analytic solution due to Rosen and Zener for a coupling with a hyperbolic secant time dependence [27], which is the electric field envelope expected from picosecond mode-locked pulses [28]. Figure 1(b) shows the envelope of an electric field auto-correlation of a single pulse as measured with a scanning Mach-Zehnder interferometer and a fast photodiode, which is consistent with the autocorrelation of a hyperbolic secant with $T_{\mathrm{pulse}} = 14.8$ ps having a linear pulse chirp of 8×10^{-3} ps^{-2}. Equation (1), however, shows that the two-photon Rabi frequency is proportional to the square of the electric field envelope. Nonetheless, sech^2 and sech are sufficiently similar that numerical solutions to the Schrödinger equation with $\Omega(t) \propto \mathrm{sech}^2[2t/T]$ match the analytic solutions with $\Omega(t) \propto \mathrm{sech}[\pi t/T]$ to within a few percent for all simulations shown here. The Rosen-Zener transition probability from an initial state $|0\rangle$ to $|1\rangle$ is [27]

$$\mathcal{P}_{0\to1} = \sin^2(\pi u)\mathrm{sech}^2[\pi\nu_{\mathrm{HF}}T_{\mathrm{pulse}}] \qquad (6)$$

for a two-photon Rabi frequency of $\Omega_{1,0}(t) = \frac{u}{T_{\mathrm{pulse}}} \times \mathrm{sech}[\frac{\pi t}{T_{\mathrm{pulse}}}]$ where u is the pulse area. Equation (6) indicates that to create a high-fidelity π pulse, the pulse duration must be many times shorter than the hyperfine period.

Figure 2(a) shows the measured transition probability as a function of pulse energy (proportional to u in Eq. (6) and monitored with a fast photodiode). Both plots in Fig. 2 were taken with a single beam path, as represented by the solid line in Fig. 1(c). The maximum transition probability of 72% corresponds [see Eq. (6)] to a pulse duration of $T_{\mathrm{pulse}} = 14.8$ ps.
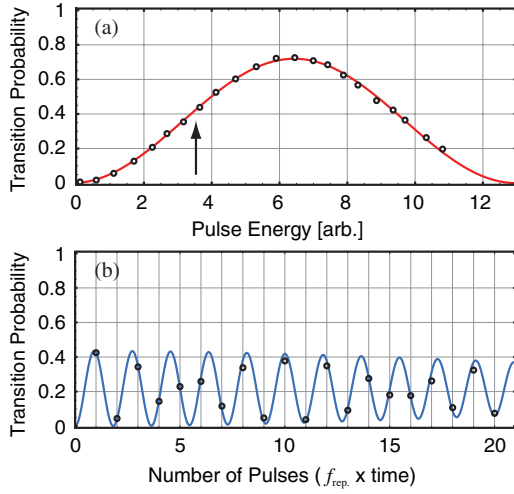
FIG. 2 (color online). (a) Qubit transition probability from a single pulse vs pulse energy. The solid curve is a fit to Eq. (6) and the peak corresponds to a pulse energy of 12 ± 2 nJ. (b) Qubit transition probability vs the number of identical (≈ 8 nJ) pulses at the laser repetition rate. The solid curve is a fit to the Rosen-Zener solution with a Gaussian contrast decay. The single pulse energy for (b) is shown with an arrow in (a).

We also studied the dynamics of a train of identical pulses [with pulse energy denoted by the arrow in Fig. 2(a)] at the laser repetition rate, shown in Fig. 2(b). The solid curve is an analytic solution including free evolution with a fitted Gaussian decay in contrast. The fitted pulse duration is $T_{\text{pulse}} = 14$ ps, in good agreement with the fitted pulse width from Fig. 2(a).

It is clear from Eq. (6) and Fig. 2(a) that for $T_{\text{pulse}} = 14.8$ ps, even with unlimited pulse energy the population transfer probability cannot exceed 72% without changing the pulse shape. In order to execute a full π pulse, we introduced a simple pulse-shaping element into the beam path in the form of a beam splitter and a delay line [18], resulting in two counterpropagating pulses as shown in Fig. 1(c). By setting the energy of each half of the pulse to transfer 50% of the population, we are able to perform a fast Ramsey experiment with a variable free-evolution time between two $\pi/2$ Raman pulses. A π pulse then corresponds to the top of a Ramsey fringe.

The results of the pulse shape delay scan are shown in Figs. 3(a)–3(c). We show results from experiments with three different polarization orientations for the two $\pi/2$ pulses. In (a), both beams drive only σ^+ transitions. The Ramsey fringes are first maximized for a delay of 72 ps, corresponding to a net π pulse after 80 ps. In the frequency domain, the shaped pulse spectrum in this case is a crude frequency comb with sinusoidal teeth separated by 14 GHz. The reason this separation is not exactly 12.6 GHz $= \nu_{\text{HF}}$ is the additional $\hat{\sigma}_z$ rotation introduced by the Rosen-Zener solution dynamics. In the limit of infinitesimally short pulses, the comb spacing would converge to ν_{HF}. Figure 3(b) shows the same experiment with

one beam driving σ^+ transitions and the other driving σ^-. The two central peaks each represent a ~ 40 ps net π pulse, which is shorter than the 80 ps pure σ^+ π pulse due to the fact that the Rabi frequency for σ^+ and σ^- transitions have opposite sign and therefore rotate the Bloch vector about different axes. Figure 3(c) shows the same experiment with orthogonal linear polarizations ("lin $\perp$ lin") where neither beam drives Raman transitions by itself.

In order to quantify the population transfer probability, we compared detection histograms [19] from a fast Raman π pulse to a π pulse applied with microwaves [29] and measured a population transfer probability of 99.3%. We also investigated the population transfer efficiency of the π pulses by repeating the gate multiple times at the laser repetition rate and monitoring the transfer probability while increasing the number of π pulses. Since the laser repetition period is very close to a half integer number of hyperfine evolution periods ($\nu_{\text{HF}}/f_{\text{rep}} \approx 104.5$), there is some natural spin-echo-type error cancellation for multiple pulses for our system. For the σ^+/σ^+ configuration, we measure a population transfer probability contrast of 91% after 25 π pulses while for σ^+/σ^- we measure 77%. Infidelity of the individual $\pi/2$ pulses will decrease the Ramsey fringe amplitude, which allows us to estimate a $\pi/2$-pulse fidelity of $>99.5\%$. Qubit rotations by arbitrary angles from 0 to π can be obtained by decreasing the pulse area and adjusting the delay time.
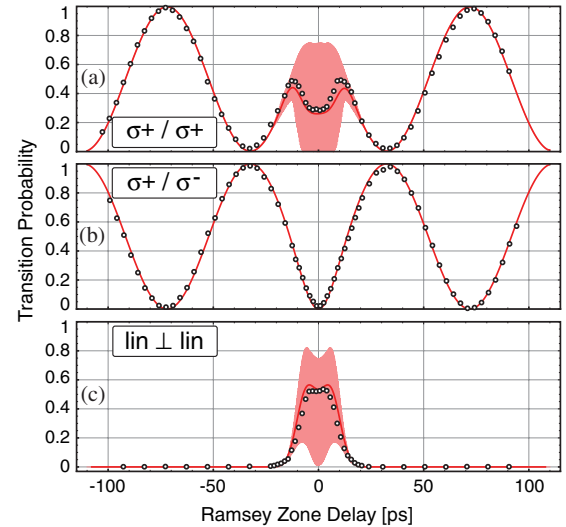

FIG. 3 (color online). Ramsey fringes for three different polarization orientations for each half of the shaped pulse obtained by fitting ensemble histograms of photon counts. The polarization configurations are (a) pure σ^+ light, (b) one is σ^+ and the other σ^-, and (c) lin $\perp$ lin. The overlap region near zero delay results in an optical standing wave with a period of 177 nm. The solid curves of (a) and (c) are calculations based on independent measurements of the optical pulse chirp and envelope with no free fit parameters. The bold curve also incorporates a thermal average of the initial ion position at the Doppler cooling limit of $\bar{n} = 40$, washing out the fine standing wave fringes.

In the overlap region (near zero delay time) in Fig. 3, the two counterpropagating $\pi/2$ pulses begin to overlap in time at the position of the atom and form an optical standing wave. For the σ^+/σ^+ and lin $\perp$ lin configurations, the two-photon Rabi frequency has 177 nm period spatial interference fringes. In the overlap regions of Figs. 3(a) and 3(c), Raman transitions are sensitive to the motion of the ion since momentum kicks of $2\hbar k$ are being transferred from the optical field. The pulse's spectrum, however, is much wider than the trap frequency (100 GHz compared to 500 kHz), so the pulse simultaneously drives many motional sidebands (including the carrier transition). For the σ^+/σ^- configuration [Fig. 3(b)], the overlap region contains linear polarization and does not drive Raman transitions.

The thin solid curves in Fig. 3 show the results of a numerical solution of the Schrödinger equation vs delay, which oscillate at optical-frequency delays of less than 1 fs in the overlap region. In this region, the ion experiences momentum kicks and phase shifts as spin states spread out in motional phase space, leaving the interferometer open. Since the final spin phase of different motional states depends sensitively on the ion's initial position, thermal averaging tends to wash out the fast spatial variation of the transition probability. The thick curves show a thermal average over the ion's initial state, assumed to be a thermal state at the Doppler cooling limit of $\bar{n} = 40$. The thin and thick curves in Fig. 3 are not fit to the data as these numerical solutions are fully constrained by the pulse duration and chirp measurements shown in Figs. 1(b) and 2(a).

Implementation of the fast cooling [14] and fast entangling gates [15,16] will require repeated spin-dependent momentum kicks generated through ultrafast interferometry in the strong excitation regime [13]. In this case, the interferometer will be closed and therefore will not be sensitive to optical wavelength interference such as the overlap region in Fig. 3(c).

We have demonstrated ultrafast single-qubit gates with a mode-locked laser pulse using an atomic qubit. For a single trapped ion, the free-evolution of the qubit can be used to perform $\hat{\sigma}_z$ rotations, and delaying the pulse arrival time will allow a rotation about an arbitrary axis in the x-y plane of the Bloch sphere. As such, the fundamental limit on the gate speed is the hyperfine period (analogous to the Larmor precession time), which would yield a gate time of ≈ 100 ps. Previous results with these same qubit levels in ^{171}Yb$^+$ have demonstrated coherence times in excess of 1000 s [2], so this single-qubit gate can be performed in a vanishingly small fraction ($<10^{-13}$) of the coherence time.

We acknowledge helpful discussions with Michael Biercuk, Ming-Shien Chang, Kihwan Kim, and Steven

*wes3000@umd.edu

[1] J. J. Bollinger *et al.*, IEEE Trans. Instrum. Meas. **40**, 126 (1991).
[2] P. T. H. Fisk *et al.*, IEEE Trans. Ultrason. Ferroelectr. Freq. Control **44**, 344 (1997).
[3] M. V. Gurudev Dutt *et al.*, Phys. Rev. B **74**, 125306 (2006).
[4] J. Berezovsky *et al.*, Science **320**, 349 (2008).
[5] K.-M. C. Fu *et al.*, Nature Phys. **4**, 780 (2008).
[6] J. R. Petta *et al.*, Science **309**, 2180 (2005).
[7] L. Viola and S. Lloyd, Phys. Rev. A **58**, 2733 (1998).
[8] D. Vitali and P. Tombesi, Phys. Rev. A **59**, 4178 (1999).
[9] L.-M. Duan and G.-C. Guo, Phys. Lett. A **261**, 139 (1999).
[10] K. Khodjasteh and D. A. Lidar, Phys. Rev. Lett. **95**, 180501 (2005).
[11] S. D. Barrettand and P. Kok, Phys. Rev. A **71**, 060310(R) (2005).
[12] S. Olmschenk *et al.*, Science **323**, 486 (2009).
[13] J. F. Poyatos *et al.*, Phys. Rev. A **54**, 1532 (1996).
[14] S. Machnes *et al.*, Phys. Rev. Lett. **104**, 183001 (2010).
[15] J. J. Garca-Ripoll, P. Zoller, and J. I. Cirac, Phys. Rev. Lett. **91**, 157901 (2003).
[16] L.-M. Duan, Phys. Rev. Lett. **93**, 100502 (2004).
[17] D. Hayes *et al.*, Phys. Rev. Lett. **104**, 140501 (2010).
[18] A. M. Weiner, Prog. Quantum Electron. **19**, 161 (1995).
[19] S. Olmschenk *et al.*, Phys. Rev. A **76**, 052314 (2007).
[20] Coherent Paladin Compact 355-4000.
[21] Fast Pulse Technology model 5046SC.
[22] D. J. Wineland *et al.*, Phil. Trans. R. Soc. A **361**, 1349 (2003).
[23] R. Ozeri *et al.*, Phys. Rev. A **75**, 042329 (2007).
[24] For Eqs. (1)–(4) we have ignored the small contributions from the $^3[3/2]^o_{3/2}$ state transition at 348 nm and neglected the difference in transition dipole moment between the $D1$ and $D2$ lines. Both effects contribute less than 15% corrections to $\Omega_{0,1}$, $\delta_0 - \delta_1$, and Γ_{spon} at 355 nm.
[25] M. J. Madsen *et al.*, Phys. Rev. Lett. **97**, 040505 (2006).
[26] Despite being slightly outside the fine-structure interval, a laser at 532 nm (=1064 nm/2) has a two-photon Rabi frequency for Ba$^+$ that is only slightly lower than Yb$^+$ at 355 nm with comparable pulse energy.
[27] N. Rosen and C. Zener, Phys. Rev. **40**, 502 (1932).
[28] A. E. Siegman, *Lasers* (University Science Books, Sausalito, CA, 1986), Chap. 28.
[29] We measure a microwave π-pulse population transfer of greater than 99.9%.